Annu. Rev. Phys. Chem. 2001. 52:255–77

TIME-RESOLVED PHOTOELECTRON SPECTROSCOPY OF MOLECULES AND CLUSTERS

Daniel M Neumark
Department of Chemistry, University of California, Berkeley, California 94720, and Chemical Sciences Division, Lawrence Berkeley National Laboratory, Berkeley, California 94720; e-mail: neumark@cchem.berkeley.edu

Key Words photoelectron spectroscopy, picosecond and femtosecond lasers, clusters, negative ions

■ **Abstract** Time-resolved photoelectron spectroscopy (TRPES) has become a powerful new tool in studying the dynamics of molecules and clusters. It has been applied to processes ranging from energy flow in electronically excited states of molecules to electron solvation dynamics in clusters. This review covers experimental and theoretical aspects of TRPES, focusing on studies of neutral and negatively charged species.

INTRODUCTION AND OVERVIEW

The past fifteen years have witnessed an explosion in the use of ultrafast lasers to follow chemical dynamics in real time with femtosecond resolution (1–3). This methodology has been applied to chemical reactions ranging in complexity from bond-breaking in diatomic molecules to dynamics in large inorganic and biological molecules, and has led to breakthroughs in our understanding of fundamental chemical processes.

Most of these experiments involve a pump-probe configuration in which an ultrafast pump pulse initiates a reaction or, more generally, creates a nonstationary state, and the evolution of this state is monitored by means of a probe pulse. The amount of information obtained from these experiments is very much dependent on the probe scheme. In condensed phase work, transient absorption is often the method of choice because of its generality. In studies of molecules and cluster in the gas phase, number densities are generally too low for transient absorption measurements, so other techniques must be used. The most popular methods, laser-induced fluorescence and resonant multiphoton ionization, require the probe laser to be resonant with an electronic transition in the species being monitored. However, as a chemical reaction initiated by the pump pulse evolves toward products, one expects the nature of the species under observation to change. Hence these probe methods are restricted to observation of the dynamics within a small region of the reaction coordinate. For example, in a seminal experiment by Zewail

& Bernstein (4) the reaction

$$H + CO_2 \rightarrow OH + CO \qquad 1.$$

was initiated by pump laser photolysis of the HI moiety in the van der Waals complex $CO_2 \cdot HI$, and the probe laser monitored OH fluorescence as a function of time. Thus, the reaction could be "clocked", in the sense that one could determine the time interval between initiation of the reaction and product formation, but not the detailed dynamics in the transition state region between reactants and products.

The development of more powerful probe methods in ultrafast experiments that could be used to monitor a reaction along the entire reaction coordinate has become a very active area in recent years. One approach is the generation of ultrafast X-ray or electron pulses to perform time-resolved X-ray or electron diffraction experiments, the goal being to be able to directly determine nuclear positions as a function of time once a reaction has been initiated (5–8). This method holds considerable promise but requires further development before it can be readily applied to chemical dynamics.

This article focuses on a different approach, time-resolved photoelectron spectroscopy, a probe methodology that has been demonstrated to be able to follow dynamics along the entire reaction coordinate and is considerably easier to implement (at present) than time-resolved diffraction experiments. In these experiments, the probe laser generates electrons through photoionization or photodetachment, and the electron kinetic energy distribution is followed as a function of time. Time-resolved photoelectron spectroscopy (TRPES) was first developed and applied to electronic dynamics on semiconductor surfaces in the mid 1980's (9) and indeed, is still a powerful tool in the investigation of metal and semiconductor surfaces (10–13). However, in this article the focus is on applications to isolated molecules and clusters, both neutral and negatively charged, in the gas phase.

TRPES experiments have been performed on neutral molecules for several years using nanosecond (ns), picosecond (ps), and femtosecond (fs) lasers to generate the pump and probe pulses. The type of dynamics one can follow depends on the temporal resolution of the laser system. TRPES experiments with ns or ps resolution have been used to probe lifetimes and radiationless decay pathways of excited electronic states. With fs resolution, experiments of this type can be done on very short-lived electronic states. In addition, one can follow a host of vibrational dynamics including dissociation, vibrational relaxation, and coherent wavepacket motion. The results of ns or ps TRPES experiments often complement information that can be obtained with other techniques such as laser-induced fluorescence and dispersed emission. Femtosecond TRPES experiments are complementary to experiments in which mass-selected ion yields are measured as a function of pump-probe delay. For example, in photodissociation, ion-yield experiments are very useful for identifying any transient species and monitoring the production of products (14), whereas TRPES provides an additional level of detail concerning the energy content of these species as a function of time.

TRPES experiments have also been performed on mass-selected negative ions. While the more complex sources and lower number densities in negative ion experiments present challenges absent in the neutral experiments, detachment energies are generally significantly lower than ionization energies in neutral species, so it is easier to generate probe laser pulses with sufficient energy to eject an electron. In addition, studies of clusters are straightforward in negative ion experiments because the ions can be mass-selected prior to their interaction with the laser pulses; analogous neutral studies require collecting photoions in coincidence with photoelectrons so that the identity of the ionized species can be ascertained.

In a typical instrument for a gas phase experiment, a skimmed neutral molecular beam or mass-selected negative ion beam interacts with pump and probe laser pulses in the interaction region of a photoelectron (PE) energy analyzer. Because these experiments involve pulsed lasers, time-of-flight electron energy analyzers have been used in virtually every time-resolved PE experiment to date. High collection efficiency analyzers are particularly useful to increase the data acquisition rate; parabolic reflectors (15) or more commonly, "magnetic bottle" analyzers (16, 17) with a collection efficiency of 50% or better have been incorporated into many of the instruments currently in use. The recent development of high power femtosecond lasers with repetition rates of 1 kHz or higher has also greatly facilitated time-resolved PE experiments with femtosecond temporal resolution. The combination of photoelectron spectroscopy and femtosecond lasers is particularly appealing because the energy resolution of electron energy analyzers (10–100 meV) is comparable to the energy spread of femtosecond laser pulses (20–30 meV for a 100 fs pulse).

An example of the principle and power of time-resolved PES is shown in Figure 1, in which femtosecond lasers (80–120 fs wide) are used to probe the dissociation of the negative ion I_2^- on its $A'^2\Pi_{g,1/2}$ excited state (18, 19). In this experiment, a pump pulse at 780 nm excites I_2^- from its ground $X^2\Sigma_u^+$ state to the repulsive $A'^2\Pi_{g,1/2}$ state. The pump pulse creates a localized wavepacket that evolves toward $I + I^-$ products. The evolution of this wavepacket is monitored by electron photodetachment with a pulse at 260 nm, and the resulting photoelectron spectrum is measured as a function of pump-probe delay. At each delay, the PE spectrum represents a Franck–Condon (FC) mapping of the dissociating–wavepacket onto the various I_2 potential energy curves, thereby providing a series of "snapshots" of the wavepacket as it moves from the initial region of excitation to asymptotic products.

Two sample PE spectra at delay times of 70 and 320 fs are shown. In the 70 fs spectrum, dissociation on the $A'^2\Pi_{g,1/2}$ state is underway but not complete. As a consequence, the PE spectrum reflects the FC overlap of the excited state wavepacket with the vibrational eigenstates supported by the various I_2 potential energy curves, and it therefore has the appearance of a molecular PE spectrum. By 300 fs, dissociation is essentially complete, and the PE spectrum represents photodetachment of the I^- photoproduct to the well-separated $^2P_{3/2}$ and $^2P_{1/2}$ spin-orbit states of the I atom. The FPE spectra of I_2^-, discussed in more detail later in

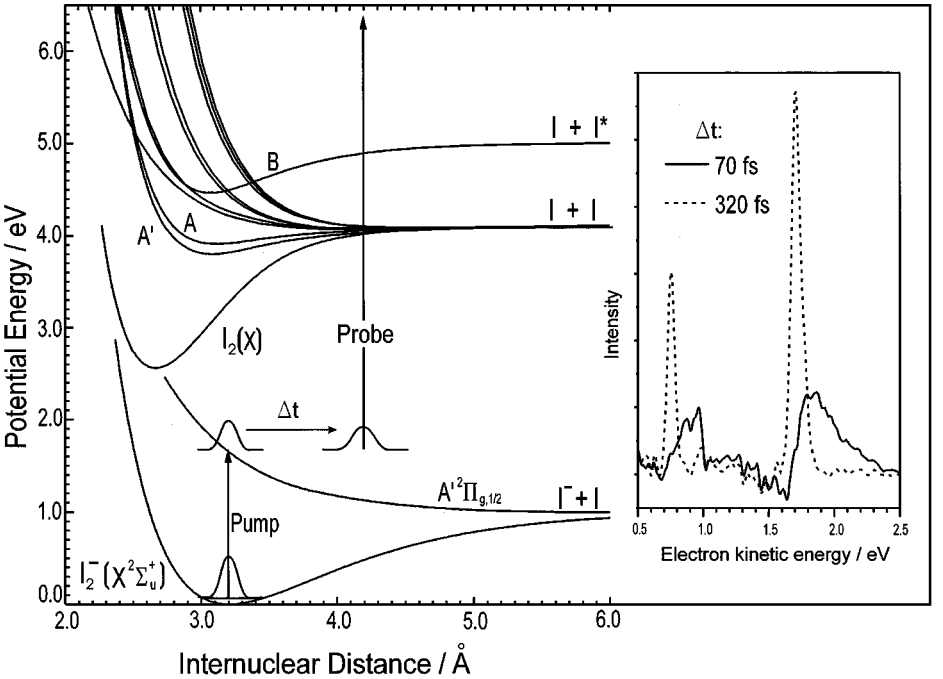

Figure 1 Time-resolved photoelectron spectroscopy of I_2^-. Relevant potential energy curves for I_2^- and I_2 are shown, along with PE spectra taken at pump-probe delay times of 70 and 320 fs.

this article, thus illustrate a simple yet fundamental process, namely the breaking of a chemical bond. They also emphasize several general advantages of TRPES: (*a*) one can indeed monitor evolution of the excited state dynamics along the entire reaction coordinate, and (*b*) the probe laser does not have to be tuned, since the PE spectrum at each delay provides the full FC mapping of the evolving wavepacket onto those electronic states accessible by photodetachment (or photoionization, in the case of neutrals).

In several time-resolved ionization experiments, zero-electron-kinetic-energy (ZEKE) spectroscopy rather than fixed-frequency PE spectroscopy was used to analyze the electrons produced by the probe pulse. ZEKE spectroscopy (20) offers considerably better resolution (0.1 meV) than PE spectroscopy but requires a tunable probe laser. This causes some experimental difficulties when dealing with ultrafast (particularly fs) lasers. In addition, while PE spectroscopy yields a complete FC mapping of the evolving state at a single probe wavelength, the equivalent information from a ZEKE experiment requires taking data at many probe wavelengths, negating the multiplexed energy analysis offered by PE spectroscopy. Moreover, while the additional energy resolution of ZEKE spectroscopy is useful in ps experiments, since the linewidths of ps lasers are typically a few

wavenumbers, this advantage is lost in fs experiments. For these reasons, relatively few time-resolved ZEKE studies have been carried out; these are discussed below along with TRPES experiments.

With this overview in mind, the rest of this article reviews past progress in the field of TRPES. Studies of neutral molecules and clusters are considered first, followed by a discussion of negative ion experiments. Theoretical treatments of both classes of experiments are discussed. Finally, experimental and theoretical developments in the area of time-resolved photoelectron angular distributions are considered.

STUDIES OF NEUTRAL MOLECULES AND CLUSTERS

In this section, TRPES experiments with nanosecond and picosecond lasers are discussed first, followed by femtosecond PES studies. This division, while somewhat arbitrary, is approximately chronological and also serves to emphasize how the nature of the dynamics that can be probed depends on the laser pulse length.

The first gas phase TRPES experiments were demonstrated in the 1980's. Using either 2 ns or 5 ps laser pulses, Pallix & Colson (21) measured the photoelectron spectra from one-color 1+2 resonant multiphoton ionization of sym-triazine via the excited $^1E''$ state. Although these were not pump-probe experiments, the photoelectron spectra showed a clear dependence on the width of the laser pulse; spectra using the ps laser showed two broad peaks, while in those obtained with the ns laser, the peak at higher electron kinetic energy (eKE) was much diminished in intensity. These observations were explained in terms of intersystem crossing (ISC) from the initially excited $^1E''$ state, responsible for the higher energy peak, to the lowest triplet (T_1) state, on a timescale between 2 ns and 5 ps. The first pump-probe time-resolved PES experiment was performed by Sekreta & Reilly (22) on benzene using ns laser pulses. In these experiments, the pump laser excited the 6_0^1 level of the $^1B_{2u}$ state. The pump-probe spectra showed the contribution of this state to the PE spectrum diminishing with time while a peak at lower eKE grew in on a time scale of $\sim$50 ns. These results were attributed to ISC from the $^1B_{2u}$ state to the lower-lying $^3B_{1u}$ (T_1) state.

These two experiments illustrate several principles of time-resolved PES as applied to radiationless transitions. First, optically dark states (the T_1 states in these examples) are detected as easily as optically allowed excited states. Hence, one can track ISC and other radiationless processes that might occur subsequent to electronic excitation. In addition, although total energy is conserved in radiationless transitions, the photoelectron spectra of the excited singlet and triplet states are easily distinguished from one another. This occurs because the difference in electronic term values between the initial and final states generally appears as vibrational excitation in the lower energy state. As long as changes in geometry upon ionization from either state are relatively small, which is often the case for aromatic molecules, FC factors dictate that $\Delta v = 0$

transitions dominate the PE spectra from both states. Hence, vibrational energy is approximately conserved upon ionization, and the bands in the PE spectra are separated by the difference in the electronic term energies.

Starting in 1990, other applications of time-resolved PES were developed. In experiments performed with picosecond lasers, Reilly (23), Knee (24), and their co-workers showed that time-resolved PES could be used to follow intramolecular vibrational relaxation (IVR) in excited electronic states. In IVR, the vibrational character of the initially excited vibronic level evolves with time, but the molecule remains in the same electronic state. In Reilly's experiments, the $^1B_2 \leftarrow {}^1A_1 1_0^1$ transition was pumped, and vibrational structure in the photoelectron spectrum in the band associated with ionization of the $^1B_2$ state exhibited a distinct time-dependence due to mixing of the $v_1 = 1$ level with the low-frequency vibrational modes associated with the alkyl chain. This result, while consistent with previous fluorescence studies by Smalley (25) and Zewail (26) nicely demonstrated how IVR could be readily distinguished from electronically nonadiabatic transitions in time-resolved PES; IVR is manifested as changes in vibrational structure within a single photoelectron band, as distinct from electronically nonadiabatic transitions in which new bands appear.

In picosecond ZEKE experiments by Knee and coworkers on fluorene (24), quantum beats were observed at a low level of vibrational excitation (800 cm^{-1}) in the S_1 state, and irreversible IVR was seen when higher vibrational levels ($\sim$ 1700 cm^{-1}) were excited. The signature of IVR was quite clear as the ZEKE spectrum evolved from a relatively sparse band at early time to a more extended and congested band by 500 ps. In related experiments on the aniline $\cdot$ CH_4 van der Waals complex (27), both IVR and predissociation were followed as a function of time and of vibrational excitation in the S_1 state of the aniline chromophore. This group also applied picosecond ZEKE spectroscopy to the S_1 state of benzene to distinguish between IVR within the S_1 state and electronic relaxation to the lower-lying T_1 and S_0 states (28).

While the above studies focused on dynamics of the S_1 state in aromatics, Weber and co-workers (29, 30) used picosecond PES to investigate electronic state mixing and internal conversion (IC) dynamics in higher-lying singlet states, in particular the S_3 and S_4 states of azulene and the S_2 state of phenanthrene, all of which exhibited IC to lower lying singlet states. Weber has also used picosecond PES to follow ISC from the S_1 state in aniline and 2- and 3-aminopyridine, finding in all cases that only the T_1 state was populated even though higher-lying triplet states were accessible (31).

Syage (32, 33) demonstrated that picosecond time-resolved PES could be used to follow reactions and solvation dynamics within clusters, the first example of a particularly powerful application of the technique. This experiment was applied to excited state proton transfer in phenol$\cdot(NH_3)_n$ clusters. The phenol chromophore is electronically excited with a 266 nm pump pulse, and proton transfer to the solvent molecules occurs, resulting in a $PhO^- \cdot\cdot H^+(NH_3)_n$ transient species in which the NH_3 molecules rearrange to better solvate the proton. Although some

of these dynamics were inferred previously from time-resolved ionization mass spectrometry on these and naphthol·$(NH_3)_n$ clusters (34–36), time-resolved PES yields a more detailed picture. In particular, the PE spectra of the n = 5 cluster showed a transient feature appearing on a time scale of 50 ps followed by a shifting of this feature toward higher eKE on a time scale of 300 ps; these observations were attributed to proton transfer and solvation, respectively.

In other applications of picosecond TRPES, de Lange and co-workers used picosecond TRPES to follow dissociation in the repulsive *A* band of CH_3I (37) and to measure lifetimes of the predissociative $\tilde{B}^1E''$ and $\tilde{C}'^1A_1'$ Rydberg states of NH_3 (38). Fischer and co-workers (39–41) used this method to measure lifetimes of several vibrational levels of the *B*, *C*, and *D* excited electronic states of the allyl radical, all of which lie about 5 eV above the ground state. The PE bands associated with the excited states disappeared on a time scale of 7–20 ps, with no other bands growing in. The observed decays were therefore attributed to IC to the allyl ground state, which could not be ionized with the probe pulse. The variation of decay rates with excitation energy approximately followed the density of ground state vibrational levels, further supporting the proposed mechanism.

The first experiments at femtosecond time resolution incorporating electron energy analysis were reported in the mid-1990s. Gerber (42), Stolow (43, 44), and their co-workers applied femtosecond ZEKE spectroscopy to vibrational wavepacket dynamics in Na_3 and I_2, respectively while Cyr & Hayden (45) used femtosecond TRPES to investigate the dynamics of internal conversion in 1,3,5-hexatriene. Gerber used a femtosecond pump pulse to create a superposition of vibrational levels in the *B* state of Na_3, and measured both total ion and ZEKE electron yield as a function of pump-probe delay. Both spectra showed clear recurrences due to coherent wavepacket dynamics on the *B* state. Stolow's experiments applied to the I_2 *B* state were similar in principle but more extensive. They yielded beautiful oscillatory structure, the phase of which varied with probe wavelength, and which showed dephasing and rephasing characteristic of wavepacket motion in an anharmonic potential.

In Hayden's work, the S_2 state of 1,3,5-hexatriene was excited, and a combination of time-resolved ion yield and PE spectroscopy measurements was used to unravel the ensuing dynamics. The PE spectra for the *cis* isomer showed very rapid ($\sim$20 fs) internal conversion from the S_2 to S_1 state, followed by IVR within the S_1 state on a time scale of 300 fs. The ion yield measurements indicated lifetimes of 750 and 270 fs for the S_1 states in the *cis* and *trans* isomers, respectively, with respect to IC to the ground electronic state. This experiment represents a clear example of how TRPES can follow very fast dynamics involving multiple electronic states.

These first fs-resolved experiments were soon followed by a flurry of related activity in other laboratories, including the first TRPE experiments by Neumark (18) on negative ions (see following section) and experiments by Chen (46) and Baumert (47) on NO and Na_2, respectively. These and all subsequent experiments used PE rather than ZEKE detection of the electrons.

The work by Baumert and co-workers (47) on Na_2 exemplifies the multiplexed nature of femtosecond PE experiments. The principle of the experiment is shown in Figure 2*a*. Two-photon excitation was used to create a wavepacket on the excited $2^1\Pi_g$ state of Na_2, and the PE spectrum after ionization with a probe pulse was measured. The eKE changes with the phase of the wavepacket because of the difference between the potentials for the $2^1\Pi_g$ state and the $X^2\Sigma_g^+$ state of Na_2^+, with higher (lower) eKE at the inner (outer) turning point. As a result, a plot of

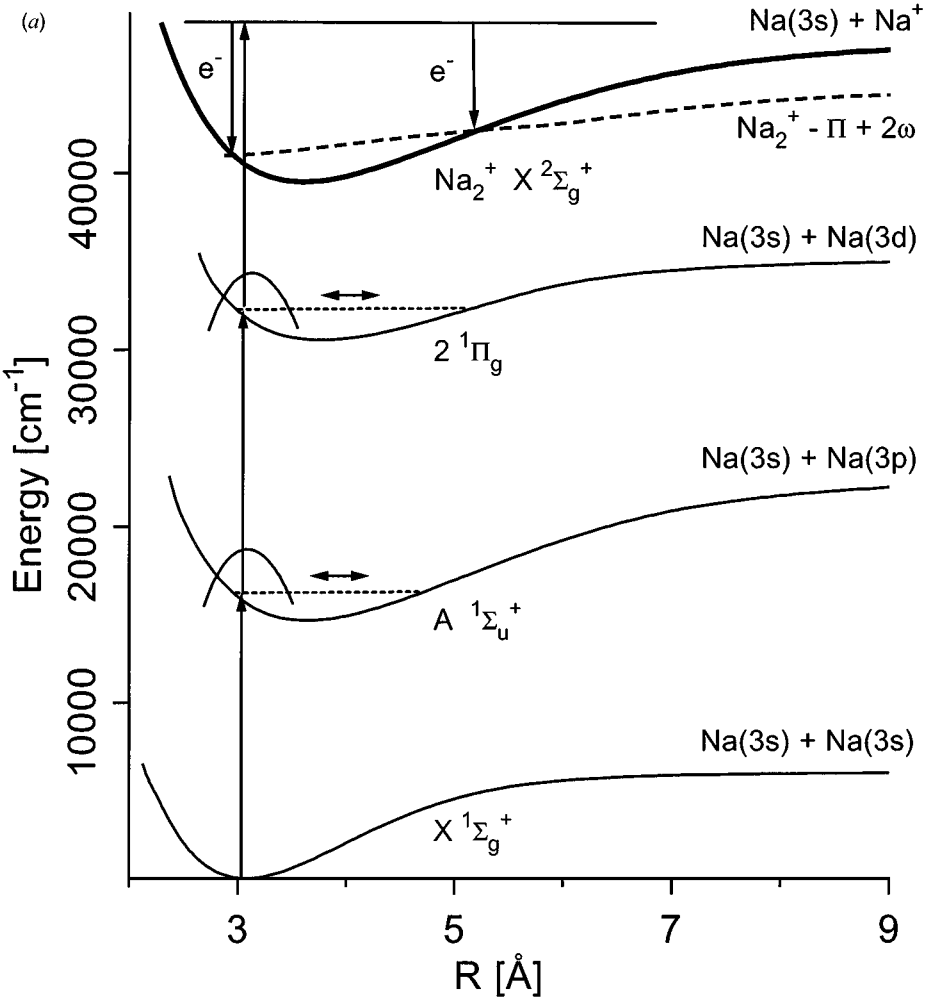

Figure 2 Femtosecond PE spectroscopy of Na_2. Potential energy curves of Na_2 and Na_2^+ are shown in (*a*), while PE spectra showing coherent wavepacket motion on the excited Na_2 states are shown in (*b*). Adapted from Reference (47).

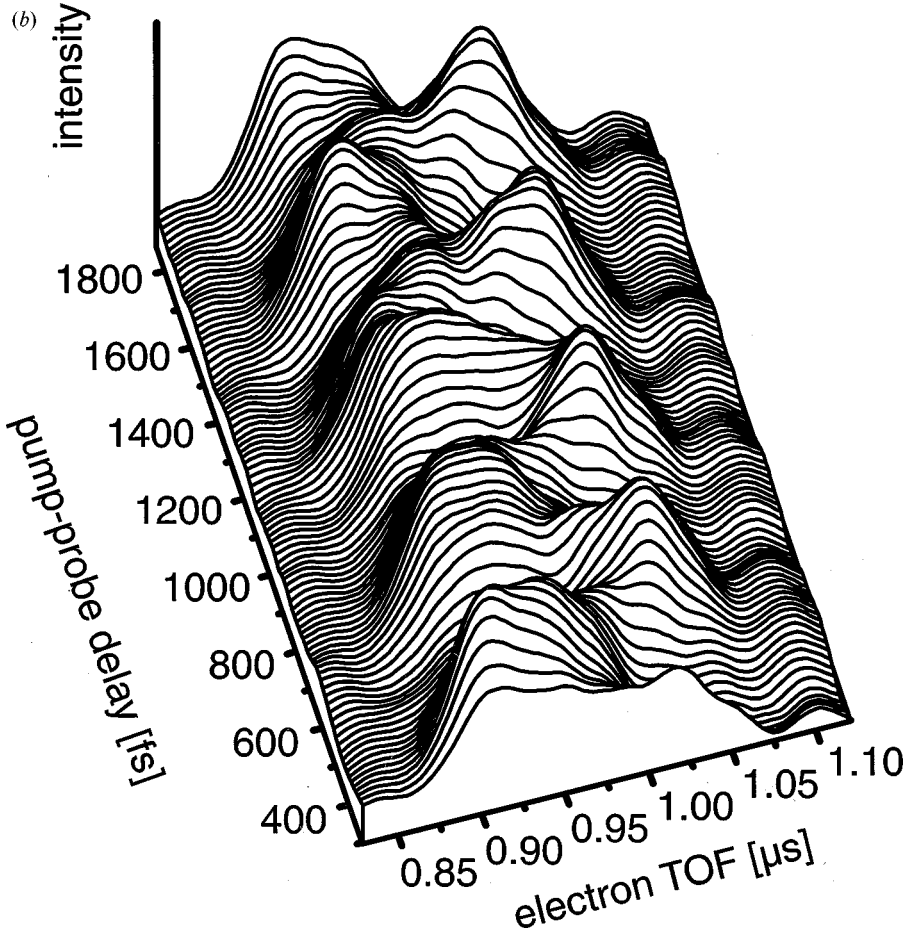

Figure 2 (*Continued*)

the photoelectron spectra versus time Figure 2*b* shows the complete excited state wavepacket dynamics. Note that a wavepacket is also created on the lower-lying $A^1\Sigma_u^+$ state through absorption of one pump photon, but because the $2^1\Pi_g \rightarrow A^1\Sigma_u^+$ transition was resonant with the pump laser, two-photon ionization out of the $A^1\Sigma_u^+$ occurs only at the inner turning point. The experimental results are in good agreement with an earlier theoretical treatment by Meier & Engel (48) and nicely complement the time-resolved total ion yield experiments by Schreiber & Wöste (49, 50).

Chen's work on NO (46) was the first in which intensity effects on time-resolved PE spectra were investigated. The experiment was in principle quite straightforward: measurement of the pump-probe photoelectron spectrum from

$2 + 1$ ionization of NO through its $C^2\Pi$ Rydberg state. At low intensity, the PE spectra with a 400 fs pump-probe delay was dominated by a single peak corresponding to the $\Delta v = 0$ transition from the $v = 0$ level of the C state. At higher pump intensities (10^{13} W/cm^2), a second feature appeared that was not resonant with any ionization transition. This feature was attributed to the $v = 3$ level of the $A^2\Sigma^+$ state being ac-Stark-shifted about 200 meV by the pump pulse into near-resonance with the C ($v = 0$) level and then returning to its zero-field value after the pump pulse terminated. More complex Stark-shifting and state mixing involving the nearby $B^2\Pi$ state were observed in the PE spectra at zero pump-probe delay.

Related experiments in which the probe laser intensity was varied were carried out by Baumert (51) on Na_2, showing enhanced contributions from ionization out of the $A^1\Sigma_u^+$ state to the femtosecond PE spectra at high probe powers. This was attributed to perturbations of the A and $2^1\Pi_g$ states of Na_2 by the probe pulse, so that the transition between the two states was near-resonant with the probe photon energy over the entire range of bond distances spanned by the wavepacket on the $A^1\Sigma_u^+$ state, as opposed to the inner turning point only (see above). Note that atomic and molecular PE spectra taken at even higher photon intensities show a whole new class of processes, such as above threshold ionization and tunneling/barrier suppression ionization. These "strong field" effects are outside the scope of this article and have been reviewed elsewhere (52).

Following the work of Hayden (45), several other groups have used femtosecond TRPES to follow very fast nonradiative decay dynamics in excited electronic states. For example, Stolow's group investigated the dynamics of $(NO)_2$ following electronic excitation at 210 nm (53). The parent $(NO)_2^+$ ion signal decayed with a time constant of 322 fs. In the absence of other information, this decay might be attributed to dissociation. However, time-resolved PE spectra showed a sharp peak associated with ionization of the NO ($A^2\Sigma^+$) photoproduct growing with a considerably slower time-constant of 730 fs. Hence, there appears to be an intermediate electronic state of the dimer that is dark with respect to photoionization at the probe wavelength (287 nm). This group also studied $S_2 \rightarrow S_1$ IC dynamics in decatetraene (54). Although the two excited states are nearly degenerate, photoionization of the S_2 state can access the cation ground state by a one-electron transition, whereas photoionization of the S_1 state leads primarily to an excited cation state lying 1.2 eV higher. Hence, the S_2 and S_1 states are readily distinguished in TRPE spectroscopy which shows that IC between the two excited states occurs on a time scale of 386 fs. Related work on the decay rates of the S_2 states in benzene, phenol and pyrazine has been reported by Radloff et al (55), Weber (56), and Stert et al (57), respectively.

Femtosecond TRPES has also been used to study dynamics in clusters. Soep and co-workers (58) examined the excited state double proton transfer reaction in the 7-azaindole dimer, comparing PE spectra obtained by $1 + 1$ ionization with 0.8 ps and 5.0 ps laser pulses. They found significantly higher PE yield with shorter pulse ionization, indicating a subpicosecond excited state lifetime consistent

with previous time-resolved ion yield measurements by Zewail and co-workers (59).

The 7-azaindole dimer is a very stable species, due to its double hydrogen bond, and can be generated as the dominant species in a free jet expansion. This is not the case for most neutral clusters, however, and to ensure that photoelectrons come from a cluster of particular size, it is desirable to collect photoelectrons in coincidence with ions. The first time-resolved coincidence experiment of this type, performed by Radloff et al (55) compared the excited state dynamics of benzene dimer with those of the monomer. They found that the decay of the S_2 to S_1 states was very rapid for both species (about 50 fs), whereas the $S_1 \rightarrow S_0$ IC decay was significantly faster in the monomer than in the dimer, 7.6 versus 100 ps. Measurement of the PE spectra made it straightforward to distinguish the two processes; $S_2 \rightarrow S_1$ IC was indicated by changes in the shape of the TRPE spectra, while $S_1 \rightarrow S_0$ IC rate was followed by the decay of the integrated PE signal. This group also investigated the dynamics of hydrogen transfer in electronically excited $(NH_3)_2$ (60). By monitoring the PE signal associated with the $(NH_3)_2^+$ and NH_4^+ ions, they were able to sort out the rather complicated dynamics associated with this system, finding time constants of 170 fs for the decay of $(NH_3)_2^*$ to $NH_4 \cdot NH_2$, and 4 ps for dissociation of the latter complex to $NH_4 + NH_2$.

Two recent important experimental developments in TRPES are likely to play a major role in the near future. Suzuki et al (61) have applied femtosecond time-resolved photoelectron imaging to ISC from the S_1 state of pyrazine. In this experiment, the electron distribution is imaged onto a position-sensitive detector, enabling one to follow the time-dependence of the photoelectron angular distribution as well as the energy distribution, and indeed Suzuki observed changes in the photoelectron angular distribution accompanying ISC. Davies et al (62) have developed an even more sophisticated experiment in which the electrons and ions produced from the pump and probe lasers are collected in coincidence and imaged. This instrument was used to follow dissociative multiphoton ionization of NO_2. At each delay time, one can measure how the electron kinetic energy varies with fragment recoil energy, thereby providing a very detailed picture of the excited state dissociation dynamics.

The other key development is the incorporation of femtosecond laser pulses with photon energies in the vacuum ultraviolet and beyond into TRPES experiments. The choice of neutral systems studied with TRPES has been limited by the requirement of a low-lying electronic state accessible via the pump pulse, and more importantly, the preference to be able to ionize the excited electronic state and its decay or dissociation products with a single probe photon. Femtosecond laser wavelengths around 200 nm have been achieved through fourth harmonic generation in nonlinear crystals, but in order to go beyond this one has to generate higher harmonics in pulsed free jets of rare gas atoms or in optical fibers (63). Recently, Sorensen et al (64) have performed TRPES on a high Rydberg state of C_2H_2 using the 6^{th} harmonic (9.42 eV) of a Ti:sapphire laser as the pump pulse. Even higher harmonics have been incorporated into TRPES experiments

by the Leone group. These were used as the probe pulse to follow the dissociation of Br_2 in real time. As these techniques become more commonplace, the range of applicability of TRPES will be increased significantly.

TRPES OF NEGATIVE IONS

Most of the neutral TRPES experiments described above have focused on radiationless, nondissociative decay in electronically excited states. Excited state dynamics are also probed in negative ion experiments, although the specific problems have been quite different, including photodissociation of bare and solvated ions, autodetachment dynamics, and electron solvation dynamics in clusters. In contrast to neutrals, experiments on negative ion clusters are straightforward in principle because the ions can be size-selected prior to interacting with the laser pulses. In addition, because detachment thresholds for negative ions are significantly lower than neutral ionization potentials, one can probe ground state dynamics induced by the pump pulse (or pulses) in negative ion experiments, whereas ground state ionization has generally been out of range in neutral TRPES experiments.

The first TRPES on a negative ion was performed with femtosecond laser pulses on I_2^-, in which the $A'^2\Pi_{g,1/2} \leftarrow X^2\Sigma_u^+$ transition (Figure 1) was pumped and the resulting dynamics on the repulsive upper state was probed (18). While the original study showed dissociation to be complete by 300 fs, as signified by the appearance of peaks associated with I^- photodetachment, subsequent work at higher electron energy resolution showed that the I^- peaks shifted 10 meV toward higher eKE from 320–720 fs (19). This was attributed to an attractive well at long range on the $A'^2\Pi_{g,1/2}$ state potential due to the charge-polarizability interaction between the separating I and I^- fragments. From these data an accurate potential for the $A'^2\Pi_{g,1/2}$ was obtained.

One also obtains information on ground state spectroscopy and dynamics from these experiments. In the process of exciting the $A'^2\Pi_{g,1/2} \leftarrow X^2\Sigma_u^+$ transition, the pump pulse generates a wavepacket on the $\tilde{X}^2\Sigma_u^+$ state of I_2^- composed primarily of the $v = 0$ and 1 states by resonant impulsive stimulated Raman scattering (RISRS) (66). Wavepacket motion appears as oscillatory structure at particular electron energies in the time-dependent PE spectra; from these oscillations the vibrational frequency of the anion, 110 ± 2 cm^{-1}, is obtained (67). This oscillatory structure persists long after the upper state dissociation dynamics are over, making it straightforward to distinguish ground and excited state dynamics. As in Baumert's experiments on Na_2 (47), different electron kinetic energies correspond to different phases of the wavepacket motion.

While the RISRS experiment probes vibrational motion only near the minimum of the $I_2^-(X^2\Sigma_u^+)$ ground state, one can access much higher vibrational levels, up to within 2% of the dissociation limit, in a three-pulse, pump-dump-probe experiment, in which the pump and dump pulses create a superposition of ground state vibrational levels via femtosecond stimulated emission pumping (SEP) (68).

The excitation energy of the wavepacket is varied by tuning the dump pulse. The wavepacket oscillates between the inner and outer turning points of the ground state potential, and these oscillations are readily detected through measurement of the photoelectron spectrum with a femtosecond probe pulse (at 263 nm) at a series of delay times. As the excitation energy is increased, the oscillation frequency drops, and the anharmonicity (measured by the rephasing time of the oscillations) increases. By measuring the frequency and anharmonicity as a function of excitation energy, a high quality potential for the I_2^- ground state was developed that should be accurate all the way up to the dissociation limit.

The above work on the ground and excited states of bare I_2^- was complemented by studies of how the excited state dynamics and ground state spectroscopy of I_2^- are affected by clusters with a weakly interacting solvating species (Ar) and a more strongly interacting solvent (CO_2). Based on previous experimental work by Lineberger (69–71), and molecular dynamics simulations by Parson (72–75), and Coker (76, 77), the excited state dynamics are strongly affected by solvation. Instead of undergoing direct dissociation on the A' state, the recoiling fragments interact with the surrounding solvent species, resulting in recombination, vibrational relaxation, and solvent evaporation. The femtosecond PE spectra enable one to follow these dynamics in considerable detail.

Femtosecond PES studies of $I_2^-(Ar)_n$ clusters ($n = 6$–20) (78, 79) showed dissociation of the I_2^- within the cluster is complete by 300 fs. From 300 fs–1 ps, the spectra yield the number of Ar atoms interacting with the I^- fragment. At later times, recombination of I_2^- occurs in $I_2^-(Ar)_{n\geq 12}$ on both the X and A states; the latter is a weakly bound excited state lying between the X and A' states. Analysis of the spectra yields the time scale for X state vibrational relaxation and solvent evaporation. In $I_2^-(Ar)_{20}$, energy transfer from I_2^- to Ar atoms through vibrational relaxation is slightly faster than energy loss from the cluster through Ar evaporation, indicating the temporary storage of energy within Ar cluster modes.

Similar experiments were performed on $I_2^-(CO_2)_n$ clusters with n = 4–16 (80, 81). At short times (<1 ps), the PE spectra show evidence for rearrangement of the solvent molecules around the separated I and I^- fragments. At longer times, features associated with recombination, vibrational relaxation, and solvent evaporation are observed for clusters with $n \geq 6$. These dynamics occur more rapidly as the cluster size increases, and in all cases are much faster than in the Ar clusters. In addition, substantial trapping in a solvent-separated state is seen for clusters with $n > 9$; this state, in which I and I^- are trapped within the cluster but have not recombined, persists for at least 200 ps.

In order to probe the effect of solvation on the I_2^- ground state potential, excitation of coherent ground state vibrational motion via RISRS was used to measure vibrational frequencies of the I_2^- chromophore in size selected $I_2^-(Ar)_n$ and $I_2^-(CO_2)_n$ clusters to wavenumber accuracy (82). Blue shifting of the frequency occurs upon solvation, with larger shifts observed for solvation with CO_2 (i.e. 4.5 cm^{-1} for $I_2^-(CO_2)_9$). The blue-shifting in the Ar clusters appears to result from repulsive solute-solvent interactions. The situation in CO_2 clusters is more

complicated and may result from a small amount of electron delocalization into the solvent, increasing the I_2^- vibrational frequency since the highest occupied molecular orbital in I_2^- is anti-bonding. The effect of solvation on much higher vibrational levels of I_2^- was probed by using femtosecond SEP on $I_2^-(CO_2)_4$ to generate a highly excited, coherent wavepacket within a cluster (83). The FPE spectra showed significant coherent relaxation of this wavepacket over 3 ps, in which one observed oscillatory motion, the period of which decreased with time as the I_2^- chromophore lost vibrational energy to the surrounding solvent molecules.

Femtosecond TRPES was also used to study the photodissociation dynamics of polyatomic anions. The first study of this type was performed by Gantefor et al (84) on Au_3^-. When this species was excited at a photon energy of 3.0 eV, a long-lived excited state was formed that decayed to $Au^- + Au_2$ on a time scale of 1500 ps; the PE spectra showed a broad feature at early times coalescing to a narrow feature corresponding to the Au^- photoproduct. At a slightly higher photon energy (3.14 eV), dissociation was far more rapid, with both Au^- and Au_2^- formed in less than 50 ps.

A similar experiment in principle was performed on I_3^- at 390 nm (85). The FPE spectra in Figure 3 show depletion of the I_3^- reactant and growth of the I_2^- and I^- products; these are clearly distinguishable since the time-evolution of the three species occurs at different electron energy ranges. Dissociation is complete after several hundred femtoseconds. In addition, the I_2^- exhibits coherent oscillations with a period of 550 fs corresponding to $\sim$0.70 eV of vibrational excitation, or $\langle v \rangle = 67$. The oscillations dephase by 4 ps and rephase at 45 and 90.5 ps on the anharmonic I_2^- potential. The gas phase frequency of ground state I_3^- was determined from oscillations in the photoelectron spectrum induced by RISRS. The dissociation dynamics were modeled using one- and two-dimensional wavepacket simulations, from which we attributed the formation of I^- to three body dissociation to $2I + I^-$ along the symmetric stretching coordinate of the excited anion potential. The photodissociation dynamics of gas phase I_3^- differ considerably from those observed previously in EtOH solution by Ruhman (86) and Vohringer (87) using transient absorption spectroscopy. In solution, substantially less I_2^- vibrational excitation is observed ($\langle v \rangle = 12$) at time delays as short as 500 fs, and no I^- is produced except as a minor channel at 266 nm (88).

Anion TRPES experiments have also focused on electron solvation dynamics in clusters. When a halide anion is dissolved in water and many other solvents, one observes absorption bands in the ultraviolet corresponding to ejection of the excess electron into the surrounding solvent molecules (89, 90). Recently, the cluster analog of these charge-transfer-to-solvent (CTTS) bands was spectroscopically observed by Johnson (91) and Cheshnovsky (92, 93) in $I^-(H_2O)_n$ and $I^-(Xe)_n$ clusters, respectively. Excitation of the CTTS bands in solution produces solvated electrons (94), so TRPES measurements on $I^-(S)_n$ clusters (S = Xe, H_2O, NH_3, CH_3OH) were undertaken to follow the electron solvation dynamics in the finite solvent networks on these clusters subsequent to excitation of the cluster CTTS band.

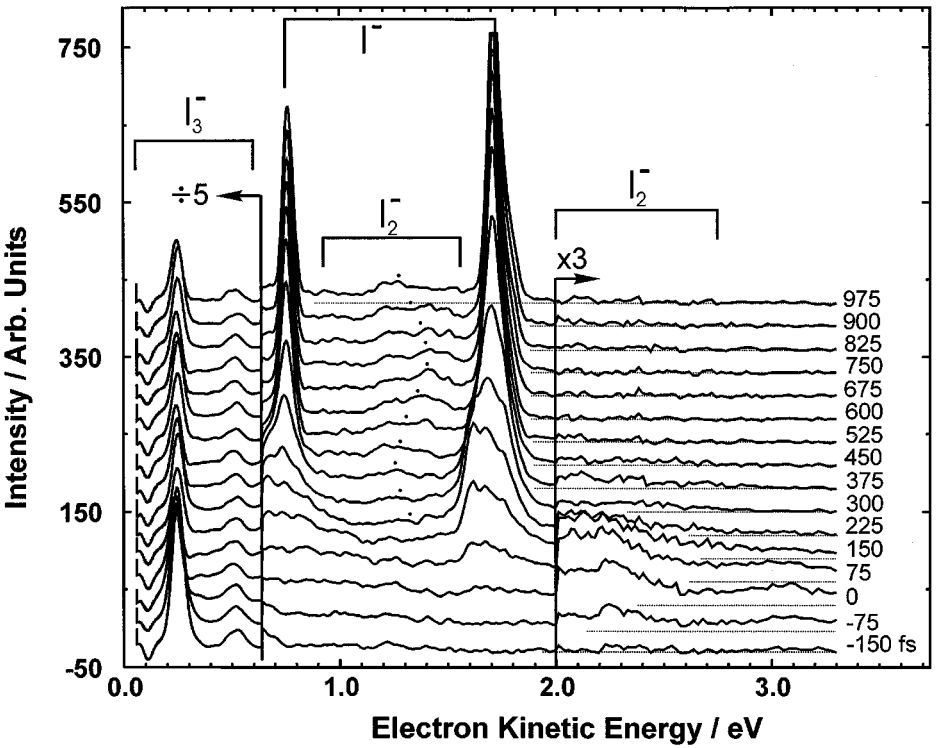

Figure 3 Femtosecond PE spectra of I_3^- using a pump and probe wavelengths of 390 nm and 260 nm, respectively. Contributions to the spectra from I_3^- reactant and the I_2^- and I^- photoproducts are indicated. Adapted from Reference (85).

In $I^-(Xe)_n$ clusters (95) the photoelectron spectra rapidly build up in intensity and then decay on a time scale that increases from 550 fs for the $n = 11$ cluster to1,550 fs for $n = 38$ cluster. The electron kinetic energy distribution does not shift with time; only the integrated intensity varies. In contrast, for the molecular solvent species H_2O, NH_3, and CH_3OH (96–98), a shift toward lower eKE by as much as 0.3 eV was observed after several hundred femtoseconds. This shift was ascribed to reorganization of the solvent network as the solvent molecules rearrange to stabilize and partially solvate the excess electron. The absence of this shift for Xe indicates that no solvent rearrangement occurs in the $I^-(Xe)_n$ clusters.

There are distinct differences among the solvent species that do show partial solvation. Clusters with NH_3 and CH_3OH show a gradual buildup of the solvation shift as the number of solvent molecules is increased from $n = 4$ to $n = 8$, whereas water clusters show no shift for $n = 4$, and the full shift of $\sim$0.3 eV occurs for clusters with $n \geq 5$. Hence, the onset of solvation appears far more abrupt in clusters with water. The lifetime of the partially solvated state is also

strongly solvent dependent. For example, in $I^-(NH_3)_{15}$, the largest NH_3 cluster studied, this state decays 53 ps, whereas a much longer decay time of 440 ps was seen for $I^-(H_2O)_8$.

Finally, Minemoto et al (99) have used TRPES to measure the lifetime of an excited state of C_3^- that lies above the threshold for autodetachment to $C_3 + e^-$. This state, first observed in a frequency-resolved experiment by Tulej et al (100), has been tentatively assigned as the $^2\Delta_u$ state and was found to have a lifetime of 2.6 ps with respect to autodetachment. Measurements of this type on larger carbon cluster anions are likely to be of significant interest given the large number of low-lying electronic states in these species.

THEORETICAL TREATMENT OF TRPES

The theoretical treatment of TRPES involves a straightforward but somewhat computationally demanding application of time-dependent quantum mechanics. In 1991, Seel & Domcke (101) wrote the first systematic theoretical paper specifically addressing TRPES and how it could be applied to follow $S_2 \rightarrow S_1$ IC dynamics in pyrazine, a problem that was not addressed experimentally until 2000 (57). In 1993, Meier & Engel (48) applied a similar treatment to TRPES of Na_2, predicting many of the features associated with coherent wavepacket motion that were later observed experimentally by Baumert (47).

Both papers described a nonperturbative treatment of the problem, the simplest version of which involves the ground state, a single excited state, and a single ionized (or detached) state. One then solves the time-dependent Schrodinger equation in the presence of the pump and probe laser fields, $E_{pu}(t)$ and $E_{pr}(t\text{-}\Delta t)$, to obtain the time-dependent wavefunction:

$$|\psi(t)\rangle = \sum_{n=0,1} \chi_n(R, t) \,|\, n\rangle + \int_0^{E_{\max}} dE_k \chi_2(R, E_k, t) \,|\, k\rangle. \qquad 2.$$

Here the $\chi_n(t)$ ($n = 0, 1, 2$) are nuclear wavefunctions associated with the ground, excited, and ionized electronic states $|0\rangle$, $|1\rangle$, and $|k\rangle$, respectively, with $\chi_2(R, E_k, t)$ the nuclear wavefunction corresponding to electron kinetic energy E_k. The photoelectron spectrum $P(E_k)$ is then given by:

$$P(E_k, \Delta t) = \lim_{t\to\infty} \int dR |\chi_2(R, E_k, t)|^2. \qquad 3.$$

In this exact treatment, the photoelectron spectrum has to be calculated for each delay time Δt and each electron kinetic energy E_k, a somewhat tedious procedure.

A considerable simplification is obtained by solving for $\chi_2(R, t)$ exactly considering the pump pulse alone, and treating the probe pulse perturbatively, as first proposed by Meier & Engel (102, 103). If $\chi_2(R, E_k, t)$ is calculated to first order

and substituted into (3), one finds (18, 102)

$$P(E_k, \Delta t) = \frac{|\mu_{12}|^2}{\hbar^2} \left| \int_{-\infty}^{\infty} dt' e^{iE_k t'} \left[\boldsymbol{e}_{pr}(t' - \Delta t) e^{iH_2 t'} \chi_1(R, t') \right] \right|^2, \qquad 4.$$

where μ_{12} is the transition dipole for photoionization or photodetachment and H_2 is the nuclear hamiltonian for the ionized or detached potential energy surface. The advantage of Equation 4 is that it generates the entire photoelectron spectrum at time delay Δt by a Fourier transform of the term in brackets. The perturbative treatment of TRPES is discussed in detail by Batista et al (104) who also propose a semiclassical method that gave excellent agreement with the full quantum mechanical treatment in simulations of the I_2^- TRPE spectra.

The assumption of a constant transition dipole for photoionization or photodetachment in all the above treatments is problematic when the state created by the pump pulse undergoes large amplitude nuclear motion or, for that matter, dissociation. Arasaki et al (105, 106) have carried out a more sophisticated calculation on the TRPES of Na_2 in which the photoionization transition amplitudes are explicitly calculated as a function of internuclear distance. In their calculation, the intermediate excited state was the $2^1\Sigma_u^+$ state of Na_2, a double-minimum state in which the character of the electronic wavefunction changes significantly on either side of the barrier; Arasaki et al. show that this affects both the photoelectron energy and angular distributions.

TIME-RESOLVED PHOTOELECTRON ANGULAR DISTRIBUTIONS

It has long been recognized in conventional (i.e. nontime-resolved) photoelectron spectroscopy that the measurement of photoelectron angular distributions provides information complementary to that obtained by photoelectron energy distributions. The angular distributions are often more difficult to interpret than the energy distributions, but they often shed light on aspects of the ionization/detachment process such as the symmetries of the electronic states involved and the presence of vibronic coupling in the ionized species. In addition, the measurement of photoelectron angular distributions can help in making assignments if two or more ionization/detachment bands are overlapped. In time-resolved experiments, there has been relatively little work on the measurement of time-resolved angular distributions compared to energy distributions, and much of this has been theoretical rather than experimental. Nonetheless it is clear from the work done so far that this type of measurement can provide significant insight into the dynamics induced by the pump pulse.

The photoelectron angular distribution from one-photon ionization of a randomly oriented ensemble of molecules is given by

$$\frac{d\sigma}{d\Omega} = \frac{\sigma}{4\pi}(1 + \beta P_2(\cos\theta)), \qquad 5.$$

where θ is the angle between the electron velocity and the polarization direction of the ionizing light. The anisotropy parameter β lies between -1 and 2 and depends on the symmetry of the initial and final states as well as the electron kinetic energy. Zare and co-workers (107) observed deviations from Equation 5 in resonant multiphoton ionization of NO because of a net alignment (or orientation) created in the intermediate electronic state through absorption of the first photon. Reid (108) was the first to show that this sensitivity of the angular distribution on the rotational wavefunction in the intermediate state could lead to time-evolution of the photoelectron angular distribution if the pump pulse in a TRPES experiment created a coherent superposition of angular momentum levels, and demonstrated this in a nanosecond-resolution experiment using this time-dependence to follow hyperfine depolarization in the NO ($A^2\Sigma^+$) state (109).

On a faster time scale, theoretical work by Reid (108, 110) McKoy (105), and Seideman (111, 112) has shown that if an ultrafast pump pulse is used to generate an aligned, coherent superposition of rotational levels, then one should observe periodicity in the photoelectron angular distribution on a picosecond time scale analogous to the recurrences seen in rotational coherence spectroscopy. Reid (113) has carried out experiments of this type through excitation and ionization of the S_1 state of para-difluorobenzene using picosecond laser pulses, although the level of vibrational excitation in the S_1 state was sufficiently high so that the time-dependent angular distributions were governed more by intramolecular vibrational energy redistribution than by pure rotational coherences.

Finally, time-dependent angular distributions measured on a femtosecond time scale can also be used to probe nonadiabatic transitions and photodissociation dynamics in polyatomic molecules following electronic excitation with ultrafast pulses. Effects of this type were seen in the TRPE imaging experiments of Suzuki (61), discussed previously, in which ISC in pyrazine was studied. Theoretical work by Seideman and co-workers (114, 115) has shown that the photoelectron angular distributions are very sensitive to changes in the shape and symmetry of the excited state electronic wavefunction associated with nonadiabatic dynamics, and these distributions should provide complementary information to energy-resolved measurements. The significance of measuring time-dependent PE angular distributions was demonstrated in an experiment performed very recently by Hayden and co-workers (116) on the photodissociation of NO_2. By measuring time-dependent photoelectron angular distributions in coincidence with NO^+ product scattered in a particular direction (parallel to the laser polarization), they could follow the evolution of the photoelectron angular distribution in the molecular frame of reference. As shown in Figure 4, the distribution evolves from a highly asymmetric distribution at short times to a forward-backward symmetric distribution by 1 ps. The short-time dynamics were attributed to the effect of the departing O atom on the electronic wavefunction of the NO photoproduct.

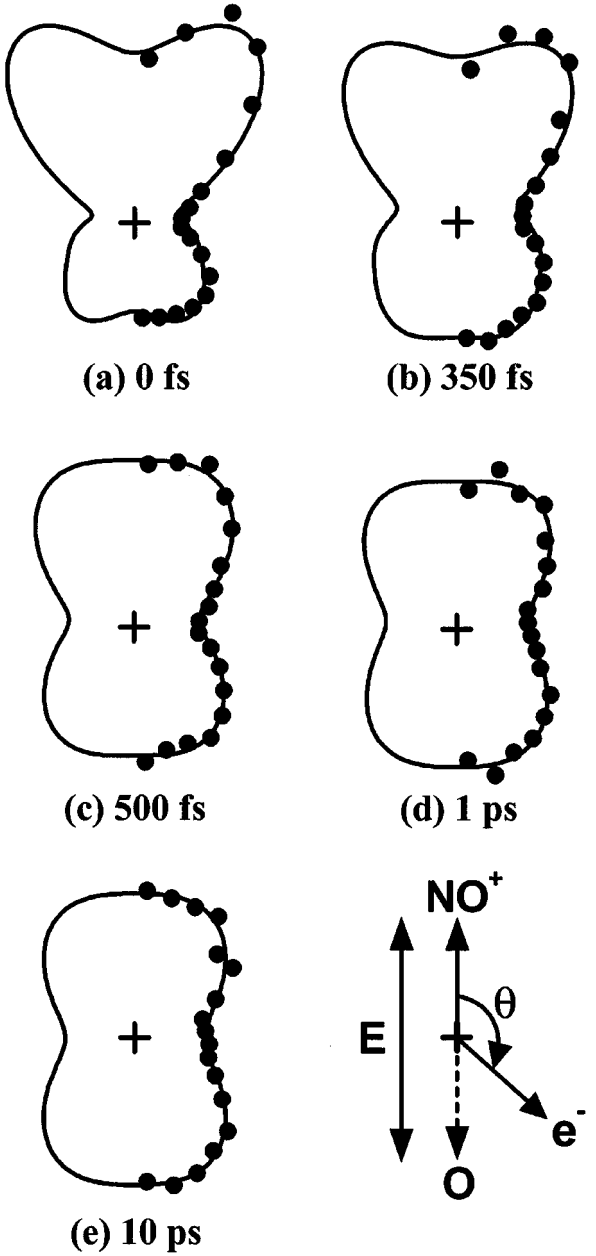

Figure 4 Time-resolved photoelectron angular distributions from NO_2 photodissociation. These are molecular frame distributions in electrons are collected in coincidence with NO^+ fragments scattered in a particular direction. Reproduced from Reference (116) with permission.

SUMMARY AND OUTLOOK

This review has presented a comprehensive discussion of time-resolved photoelectron spectroscopy as applied to gas phase molecular and cluster dynamics. A wide range of dynamical processes in neutral and negatively charged species had already been investigated using this technique, and TRPES is now recognized as a powerful new tool for the study of chemical dynamics. Two new developments described in this article hold considerable promise in the near future. First, as high harmonic generation of ultrafast laser pulses becomes more routine, it should be possible to perform TRPES of the valence electrons of many more neutral species, and also to investigate time-dependent PE spectra of the core electrons, thereby providing a complementary perspective of dissociatve and reactive processes initiated by the pump pulse. The recent incorporation of electron imaging techniques in TRPES experiments is also very appealing as it enables the measurement of time-dependent photoelectron angular distributions.

While TRPES experiments have thus far been limited to the gas phase and semiconductor or metal surfaces, there is no reason why they cannot be extended to other media. In principle, TRPES can be applied to any type of system accessible to conventional PES. For example, conventional photoelectron spectroscopy has been applied to liquid jets in order to probe structure and dynamics at the gas-liquid interface (117), and this would clearly be an interesting application of TRPES. Experiments of this type would provide a vital link with some of the cluster dynamics experiments described in this article.

ACKNOWLEDGMENTS

Support from the National Science Foundation under Grant No. CHE-9710243 is gratefully acknowledged. The author is indebted to his many co-workers on the anion femtosecond photoelectron spectroscopy project in his laboratory: B Jefferys Greenblatt, Martin Zanni, Alison Davis, Christian Frischkorn, Rainer Weinkauf, Leo Lehr, Benoit Soep, Mohammed Elhanine, Arthur Bragg, and Roland Wester.

LITERATURE CITED

1. Khundkar LR, Zewail AH. 1990. *Annu. Rev. Phys. Chem.* 41:15–60
2. Polanyi JC, Zewail AH. 1995. *Accts. Chem. Res.* 28:119–32
3. Zewail AH. 1996. *J. Phys. Chem.* 100:12,701–24
4. Scherer NF, Khundkar LR, Bernstein RB, Zewail AH. 1987. *J. Chem. Phys.* 87:1451–53
5. Williamson JC, Cao JM, Ihee H, Frey H, Zewail AH. 1997. *Nature* 386:159–62
6. Rischel C, Rousse A, Uschmann I, Albouy PA, Geindre JP, et al. 1997. *Nature* 390:490–92
7. Chin AH, Schoenlein RW, Glover TE, Balling P, Leemans WP, Shank CV. 1999. *Phys. Rev. Lett.* 83:336–39
8. Siders CW, Cavalleri A, Sokolowski-Tinten

K, Toth C, Guo T, et al. 1999. *Science* 286:1340–42
9. Haight R, Bokor J, Stark J, Storz RH, Freeman RR, Bucksbaum PH. 1985. *Phys. Rev. Lett.* 54:1302–5
10. Hertel T, Knoesel E, Wolf M, Ertl G. 1996. *Phys. Rev. Lett.* 76:535–38
11. Hofer U, Shumay IL, Reuss C, Thomann U, Wallauer W, Fauster T. 1997. *Science* 277:1480–82
12. Ge NH, Wong CM, Lingle RL, McNeill JD, Gaffney KJ, Harris CB. 1998. *Science* 279:202–5
13. Petek H, Weida MJ, Nagano H, Ogawa S. 2000. *Science* 288:1402–4
14. Pedersen S, Herek JL, Zewail AH. 1994. *Science* 266:1359–64
15. Steadman J, Syage JA. 1993. *Rev. Sci. Instrum.* 64:3094–3103
16. Kruit P, Read FH. 1983. *J. Phys. E* 16:313–24
17. Cheshnovsky O, Yang SH, Pettiette CL, Craycraft MJ, Smalley RE. 1987. *Rev. Sci. Instrum.* 58:2131–37
18. Greenblatt BJ, Zanni MT, Neumark DM. 1996. *Chem. Phys. Lett.* 258:523–29
19. Zanni MT, Batista VS, Greenblatt BJ, Miller WH, Neumark DM. 1999. *J. Chem. Phys.* 110:3748–55
20. Muller-Dethlefs K, Schlag EW. 1991. *Annu. Rev. Phys. Chem.* 42:109–36
21. Pallix JB, Colson SD. 1985. *Chem. Phys. Lett.* 119:38–41
22. Sekreta E, Reilly JP. 1988. *Chem. Phys. Lett.* 149:482–86
23. Song XB, Wilkerson CW, Lucia J, Pauls S, Reilly JP. 1990. *Chem. Phys. Lett.* 174:377–84
24. Smith JM, Lakshminarayan C, Knee JL. 1990. *J. Chem. Phys.* 93:4475–76
25. Powers DE, Hopkins JB, Smalley RE. 1980. *J. Chem. Phys.* 72:5721–30
26. Baskin JS, Dantus M, Zewail AH. 1986. *Chem. Phys. Lett.* 130:473–81
27. Smith JM, Zhang X, Knee JL. 1993. *J. Chem. Phys.* 99:2550–59
28. Smith JM, Zhang X, Knee JL. 1995. *J. Phys. Chem.* 99:1768–75
29. Weber PM, Thantu N. 1992. *Chem. Phys. Lett.* 197:556–61
30. Thantu N, Weber PM. 1993. *Chem. Phys. Lett.* 214:276–80
31. Kim B, Schick CP, Weber PM. 1995. *J. Chem. Phys.* 103:6903–13
32. Syage JA. 1993. *Chem. Phys. Lett.* 202:227–32
33. Syage JA. 1995. *J. Phys. Chem.* 99:5772–86
34. Breen JJ, Willberg DM, Gutmann M, Zewail AH. 1990. *J. Chem. Phys.* 93:9180–84
35. Kim SK, Breen JJ, Willberg DM, Peng LW, Heikal A, et al. 1995. *J. Phys. Chem.* 99:7421–35
36. Hineman MF, Brucker GA, Kelley DF, Bernstein ER. 1992. *J. Chem. Phys.* 97:3341–47
37. Dobber MR, Buma WJ, Delange CA. 1993. *J. Chem. Phys.* 99:836–53
38. Dobber MR, Buma WJ, Delange CA. 1995. *J. Phys. Chem.* 99:1671–85
39. Schultz T, Fischer I. 1997. *J. Chem. Phys.* 107:8197–8200
40. Schultz T, Fischer I. 1998. *J. Chem. Phys.* 109:5812–22
41. Schultz T, Clarke JS, Gilbert T, Deyerl HJ, Fischer I. 2000. *Faraday Discuss.* 115:17–31
42. Baumert T, Thalweiser R, Gerber G. 1993. *Chem. Phys. Lett.* 209:29–34
43. Fischer I, Villeneuve DM, Vrakking MJJ, Stolow A. 1995. *J. Chem. Phys.* 102:5566–69
44. Fischer I, Vrakking MJJ, Villeneuve DM, Stolow A. 1996. *Chem. Phys.* 207:331–54
45. Cyr DR, Hayden CC. 1996. *J. Chem. Phys.* 104:771–74
46. Ludowise P, Blackwell M, Chen Y. 1996. *Chem. Phys. Lett.* 258:530–39
47. Assion A, Geisler M, Helbing J, Seyfried V, Baumert T. 1996. *Phys. Rev. A* 54:R4605–7
48. Meier C, Engel V. 1993. *Chem. Phys. Lett.* 212:691–96
49. Rutz S, Greschik S, Schreiber E, Wöste

L. 1996. *Chem. Phys. Lett.* 257:365–73
50. Schreiber E. 1998. *Femtosecond Real-Time Spectroscopy of Small Molecules and Clusters*. New York: Springer
51. Frohnmeyer T, Hofmann H, Strehle M, Baumert T. 1999. *Chem. Phys. Lett.* 312:447–54
52. Levis RJ, DeWitt MJ. 1999. *J. Phys. Chem. A* 103:6493–6507
53. Blanchet V, Stolow A. 1998. *J. Chem. Phys.* 108:4371–74
54. Blanchet V, Zgierski MZ, Seideman T, Stolow A. 1999. *Nature* 401:52–54
55. Radloff W, Stert V, Freudenberg T, Hertel IV, Jouvet C, DedonderLardeux C, Solgadi D. 1997. *Chem. Phys. Lett.* 281:20–26
56. Schick CP, Carpenter SD, Weber PM. 1999. *J. Phys. Chem. A* 103:10,470–76
57. Stert V, Farmanara P, Radloff W. 2000. *J. Chem. Phys.* 112:4460–64
58. LopezMartens R, Long P, Solgadi D, Soep B, Syage J, Millie P. 1997. *Chem. Phys. Lett.* 273:219–26
59. Douhal A, Kim SK, Zewail AH. 1995. *Nature* 378:260–63
60. Stert V, Radloff W, Schulz CP, Hertel IV. 1999. *Eur. Phys. J. D* 5:97–106
61. Suzuki T, Wang L, Kohguchi H. 1999. *J. Chem. Phys.* 111:4859–61
62. Davies JA, LeClaire JE, Continetti RE, Hayden CC. 1999. *J. Chem. Phys.* 111:1–4
63. Durfee CG, Rundquist AR, Backus S, Herne C, Murnane MM, Kapteyn HC. 1999. *Phys. Rev. Lett.* 83:2187–90
64. Sorensen SL, Bjorneholm O, Hjelte I, Kihlgren T, Ohrwall G, et al. 2000. *J. Chem. Phys.* 112:8038–42
65. Deleted in proof
66. Banin U, Bartana A, Ruhman S, Kosloff R. 1994. *J. Chem. Phys.* 101:8461–81
67. Zanni MT, Taylor TR, Greenblatt BJ, Soep B, Neumark DM. 1997. *J. Chem. Phys.* 107:7613
68. Zanni MT, Davis AV, Frischkorn C, Elhanine M, Neumark DM. 2000. *J. Chem. Phys.* 112:8847–54
69. Papanikolas JM, Vorsa V, Nadal ME, Campagnola PJ, Buchenau HK, Lineberger WC. 1993. *J. Chem. Phys.* 99:8733–50
70. Vorsa V, Campagnola PJ, Nandi S, Larsson M, Lineberger WC. 1996. *J. Chem. Phys.* 105:2298–308
71. Vorsa V, Nandi S, Campagnola PJ, Larsson M, Lineberger WC. 1997. *J. Chem. Phys.* 106:1402–10
72. Faeder J, Delaney N, Maslen PE, Parson R. 1997. *Chem. Phys. Lett.* 270:196–205
73. Delaney N, Faeder J, Maslen PE, Parson R. 1997. *J. Phys. Chem. A* 101:8148–51
74. Faeder J, Delaney N, Maslen PE, Parson R. 1998. *Chem. Phys.* 239:525
75. Faeder J, Parson R. 1998. *J. Chem. Phys.* 108:3909–914
76. Batista VS, Coker DF. 1997. *J. Chem. Phys.* 106:7102–16
77. Margulis CJ, Coker DF. 1999. *J. Chem. Phys.* 110:5677–90
78. Greenblatt BJ, Zanni MT, Neumark DM. 1997. *Science* 276:1675
79. Greenblatt BJ, Zanni MT, Neumark DM. 1999. *J. Chem. Phys.* 111:10,566–77
80. Greenblatt BJ, Zanni MT, Neumark DM. 1997. *Faraday Discuss.* 108:101–13
81. Greenblatt BJ, Zanni MT, Neumark DM. 2000. *J. Chem. Phys.* 112:601–12
82. Zanni MT, Greenblatt BJ, Neumark DM. 1998. *J. Chem. Phys.* 109:9648–51
83. Davis AV, Zanni MT, Frischkorn C, Elhanine M, Neumark DM. 2000. *J. Electron Spectrosc. Rel. Phenom.* 112:221–30
84. Gantefor G, Kraus S, Eberhardt W. 1998. *J. Electron Spectrosc. Rel. Phenom.* 88:35–40
85. Zanni MT, Greenblatt BJ, Davis AV, Neumark DM. 1999. *J. Chem. Phys.* 111:2991–3003
86. Banin U, Ruhman S. 1993. *J. Chem. Phys.* 98:4391–4403
87. Kuhne T, Vohringer P. 1996. *J. Chem. Phys.* 105:10,788–802
88. Kuhne T, Kuster R, Vohringer P. 1998. *Chem. Phys.* 233:161–78

89. Franck J, Scheibe G. 1928. *Z. Phys. Chem. A* 139:22–31
90. Blandamer MJ, Fox MF. 1970. *Chem. Rev.* 70:59–93
91. Serxner D, Dessent CEH, Johnson MA. 1996. *J. Chem. Phys.* 105:7231–34
92. Becker I, Markovich G, Cheshnovsky O. 1997. *Phys. Rev. Lett.* 79:3391–94
93. Becker I, Cheshnovsky O. 1999. *J. Chem. Phys.* 110:6288–97
94. Jortner J, Ottolenghi M, Stein G. 1964. *J. Phys. Chem.* 68:247–55
95. Zanni MT, Frischkorn C, Davis AV, Neumark DM. 2000. *J. Phys. Chem. A* 104:2527–30
96. Lehr L, Zanni MT, Frischkorn C, Weinkauf R, Neumark DM. 1999. *Science* 284:635–38
97. Davis AV, Zanni MT, Frischkorn C, Neumark DM. 2000. *J. Electron Spectrosc. Relat. Phenom.* 108:203–11
98. Frischkorn C, Zanni MT, Davis AV, Neumark DM. 2000. *Faraday Discuss.* 115:49–62
99. Minemoto S, Muller J, Gantefor G, Munzer HJ, Boneberg J, Leiderer P. 2000. *Phys. Rev. Lett.* 84:3554–57
100. Tulej M, Fulara J, Sobolewski A, Jungen M, Maier JP. 2000. *J. Chem. Phys.* 112:3747–53
101. Seel M, Domcke W. 1991. *J. Chem. Phys.* 95:7806–22
102. Meier C, Engel V. 1994. *J. Chem. Phys.* 101:2673–77
103. Meier C, Engel V. 1994. *Phys. Rev. Lett.* 73:3207–10
104. Batista VS, Zanni MT, Greenblatt BJ, Neumark DM, Miller WH. 1999. *J. Chem. Phys.* 110:3736–47
105. Arasaki Y, Takatsuka K, Wang K, McKoy V. 1999. *Chem. Phys. Lett.* 302:363–74
106. Arasaki Y, Takatsuka K, Wang K, McKoy V. 2000. *J. Chem. Phys.* 112:8871–84
107. Leahy DJ, Reid KL, Zare RN. 1991. *J. Chem. Phys.* 95:1757–67
108. Reid KL. 1993. *Chem. Phys. Lett.* 215:25–30
109. Reid KL, Duxon SP, Towrie M. 1994. *Chem. Phys. Lett.* 228:351–56
110. Reid KL, Underwood JG. 2000. *J. Chem. Phys.* 112:3643–49
111. Althorpe SC, Seideman T. 1999. *J. Chem. Phys.* 110:147–55
112. Seideman T. 1999. *Phys. Rev. Lett.* 83:4971–74
113. Reid KL, Field TA, Towrie M, Matousek P. 1999. *J. Chem. Phys.* 111:1438–45
114. Seideman T. 2000. *J. Chem. Phys.* 113:1677–80
115. Blanchet V, Lochbrunner S, Schmitt M, Shaffer JP, Larsen JJ, et al. 2000. *Faraday Discuss.* 115:33–48
116. Davies JA, Continetti RE, Chandler DW, Hayden CC. 2000. *Phys. Rev. Lett.* 84:5983–86
117. Faubel M, Steiner B, Toennies JP. 1997. *J. Chem. Phys.* 106:9013–31